Bioorganic & Medicinal Chemistry xxx (2015) xxx–xxx

Contents lists available at ScienceDirect

Bioorganic & Medicinal Chemistry

journal homepage: www.elsevier.com/locate/bmc

Design, synthesis, and biological evaluation of amide imidazole derivatives as novel metabolic enzyme CYP26A1 inhibitors

Bin Sun, Kai Liu, Jing Han, Li-yu Zhao, Xiao Su, Bin Lin, Dong-Mei Zhao *, Mao-Sheng Cheng

Key Laboratory of Structure-Based Drug Design and Discovery, Ministry of Education, School of Pharmaceutical Engineering, Shenyang Pharmaceutical University, 103 Wenhua Road, Shenhe District, Shenyang 110016, PR China

ARTICLE INFO

Article history:
Received 24 April 2015
Revised 18 August 2015
Accepted 19 August 2015
Available online xxxx

Keywords:
All-trans-retinoic acid (ATRA)
CYP26A1
Amide imidazole derivatives
Binding model
Biological evaluation

ABSTRACT

All-trans-retinoic acid (ATRA) as a physiological metabolite of vitamin A is widely applied in the treatment of cancer, skin, neurodegenerative and autoimmune diseases. CYP26A1 enzyme, induced by ATRA in liver and target tissues, metabolizes ATRA into 4-hydroxyl-RA. Inhibition of CYP26A1 metabolic enzyme represents a promising strategy for discovery of new specific anticancer agents.

Herein, we describe the design, synthesis and biological evaluation of a series of new amide imidazole derivatives as retinoic acid metabolism blocking agents (RAMBAs) toward CYP26A1 enzyme. First, based on the recent theoretical models (Sun et al., *J. Mol. Graph. Model.*, **2015**, *56*, 10–19) a series of RAMBAs with novel scaffolds were designed using fragment-based drug discovery approach. Subsequently, the new RAMBAs were synthesized and evaluated for their biological activities. All the compounds demonstrated appropriate enzyme activities and cell activities. The promising inhibitors **20** and **23** with IC_{50} value of 0.22 μM and 0.46 μM toward CYP26A1, respectively, were further evaluated for CYP selectivity and the metabolic profile of ATRA. Both compounds **20** and **23** showed higher selectivity for CYP26A1 over other CYPs (CYP2D6, CYP3A4) when compared to liarozole. They also showed better inhibitory activities for the metabolism of ATRA when also compared to liarozole. These studies further validated the pharmacophore and structure–activity relationship models obtained about CYP26A1 inhibitors and highlighted the promising activities of the new series of CYP26A1 inhibitors designed from such models. They also paved the way for future development of those candidates as potential drugs.

Published by Elsevier Ltd.

1. Introduction

All-trans-retinoic acid (ATRA) as a physiological metabolite of vitamin A plays a crucial role in the regulation of cellular differentiation, proliferation and gene expression.[1–3] As a key signaling molecule, it is widely applied in the treatment of cancer, skin, neurodegenerative and autoimmune diseases, especially in oncology against acute promyelocytic leukemia (APL). ATRA can change the prognosis of APL from a fatal leukemia to a highly curable disease.[4–7] Unfortunately, although ATRA is useful in the treatment of cancer and skin-related diseases, its clinical applications have been severely hampered by the emergence of resistance, and the fact that the ATRA is very easy to be metabolized into 4-hydroxyl-RA by CYP26A1 enzyme.[8,9] Inhibition of CYP26A1 metabolic enzyme represents a promising strategy for the discovery of new specific anticancer agents.

In the past few years, several families of retinoic acid metabolism blocking agents (RAMBAs) targeting CYP26A1 have been described. The antimycotic substances such as ketoconazole, miconazole, itraconazole and liarozole were the first generation RAMBAs,[10–12] which were evaluated as potent blocking agents to inhibit CYP26A1 activities (Fig. 1). Unfortunately, there are adverse effects for those compounds that have been attributed to the lack of CYP26 isoform specificity. Subsequent extensive structure–activity relationship (SAR) studies on imidazole derivatives have led to the discovery of the second generation CYP26A1 inhibitors with new scaffolds, such as OSI Pharma 15c, Naphthyl compound, R115866 and R116010.[13–16] The second generation RAMBAs (Fig. 2) exhibit higher potency and better specificity against CYP26A1 than the first generation compounds, and some of them have appeared in clinical studies and have shown some encouraging preclinical and clinical results: improved specificity and activity.[17–19] Although these compounds have different scaffolds, they share three common structural characteristics: a main chain consisting of hydrophobic aromatic groups, a side chain consisting of a flexible hydrophobic fragment, and an imidazole group or triazole group. The structural characteristics can be well matched to the pharmacophore model of RAMBAs.[21]

* Corresponding author. Tel.: +86 24 2398 6413; fax: +86 24 2399 5043.
E-mail address: medchemzhao@163.com (D.-M. Zhao).

http://dx.doi.org/10.1016/j.bmc.2015.08.019
0968-0896/Published by Elsevier Ltd.

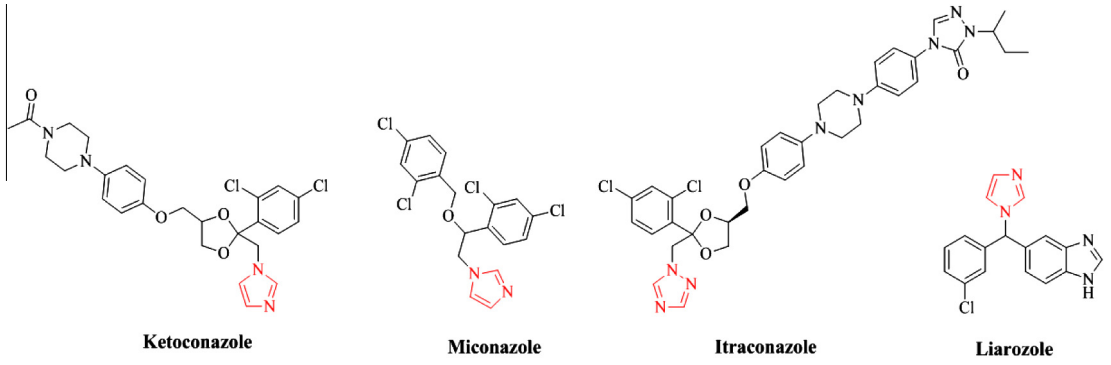

Figure 1. The first generation RAMBAs.

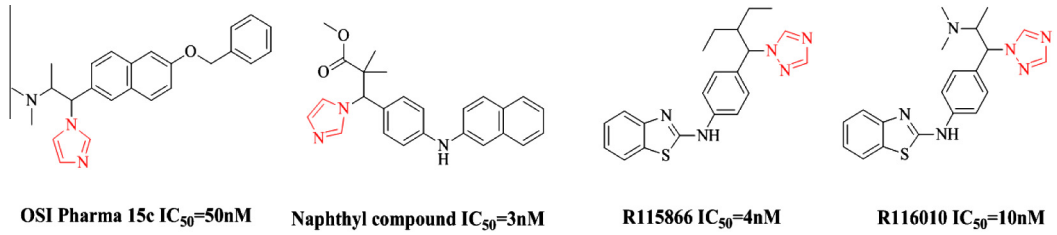

Figure 2. The second generation RAMBAs.

In recent years, fragment-based drug discovery (FBDD) approach has been playing an increasing role in the drug development.[22] Fragments with the characteristics of small molecular weight, diversified scaffold, high modifiability, are an ideal resource for drug design. In addition, the approach also pays more attention to the drug-like factors, according to the combination mode of the fragments binding with its target protein. It is then optimized to obtain good drug-like lead compounds.[23,24] Medicinal chemists can evolve, connect, integrate fragments and turn them into drug candidates through structure-based optimization. Compared to traditional drug design approach, FBDD is more suitable for lead compound discovery. It was therefore adopted to design novel RAMBAs. From the previous study,[20,21] active fragments that fit the subpockets of CYP26A1 have been identified through a combined molecular docking and pharmacophore modeling approach. In this study, FBDD method was employed to link those fragments together to design a series of novel amide imidazole derivatives as CYP26A1 inhibitors. Then they were synthesized and evaluated using biochemical and cell-based assays for their activities against CYP26A1. The results showed much improvement over the previous study carried out in our group.[33] The study provides a useful strategy for designing novel and specific RAMBAs against CYP26A1.

2. Results and discussion

2.1. The design of CYP26A1 inhibitors

Based on the detailed inhibitor–enzyme interaction model described in the previous study,[21] RAMBAs with new scaffolds were designed using FBDD approach, which was expected to have improved selectivity and specificity. The strategy was to replace the main chain and side chain groups with other active fragments (Fig. 3), which were found to occupy CYP26A1 pocket A very well by molecular docking. They were biphenyl fragment, arylpyrrole fragment, benzothiazolyl fragment and were chose as fragments of main chain groups (M) for pocket A. The novel flexible ester fragments (R) matched pocket C well and were chose for that pocket. The relatively small imidazole fragments were retained for pocket B so that the compounds would retain the essential coordinate bond with the ferrous ion in the heme group. Finally, the novel amide imidazole derivatives were constructed by connecting the main chain groups, the side chain groups and the imidazole group.

Further studies by molecular docking between the newly designed compounds and CYP26A1 enzyme demonstrated that they had similar binding modes as the representative second generation RAMBAs (Fig. 4). The docking study was carried out using Discovery Studio 3.5.[25] When they were bound to CYP26A1, the core of the aromatic main chain formed a series of interactions with the surrounding amino acid residues (Pro332 and Lys436). The nitrogen atom of the imidazole core formed the coordinate bond with the ferrous ion of the heme group in pocket B. The flexible ester side chain groups were shown to fit into pocket C very well. These compounds so designed were expected to be good RAMBAs and the following experimental data confirmed the hypothesis of our design.

2.2. Synthesis

The synthetic route of the key intermediates **2** is illustrated in Scheme 1. The commercially available starting material 4-bromobenzaldehyde was oxidized with potassium permanganate in 2 N basic condition to provide compound **1**. Next, compound **1** with phenylboronic acid and palladium acetate in refluxing dioxane afforded the white key intermediate **2**.[26]

Scheme 2 shows the synthesis of the key intermediate 5-chloro-3-methyl-1-phenyl-1*H*-pyrazole-4-carboxylic acid **6**. The starting material aniline was treated with sodium nitrite and stannous chloride under acidic conditions to provide compound **3**. Then the compound **3** was converted to compound **4** using ethyl acetoacetate in the presence of anhydrous ethanol at 75 °C for 6 h with 81% yield. Next, condensation of compound **4** with phosphorus oxychloride and *N*,*N*-dimethylformamide in refluxing conditions

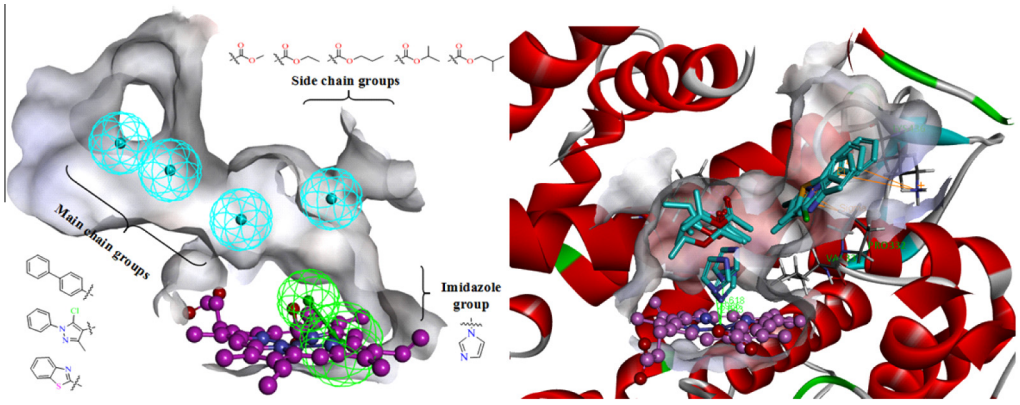

Figure 3. The combination pattern of active fragments in the subpockets of CYP26A1.

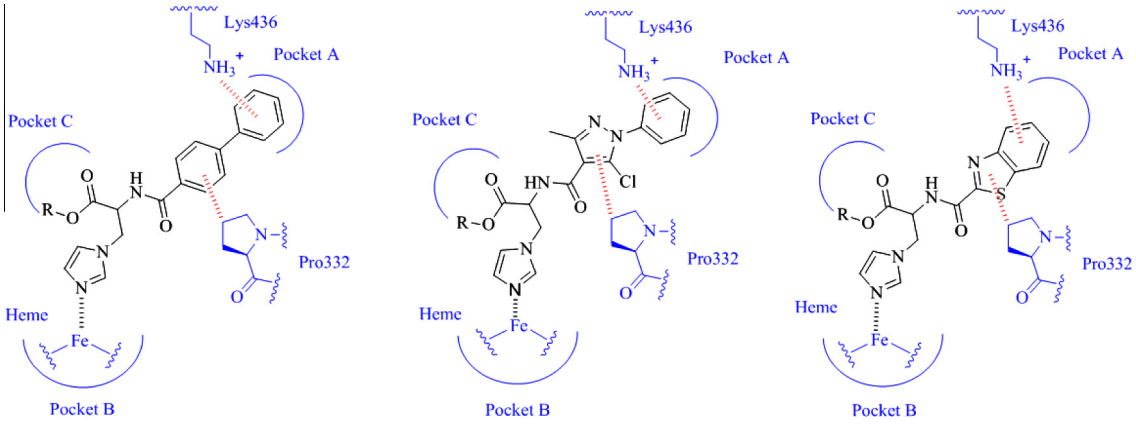

Figure 4. Design of amide imidazole derivatives as novel metabolic enzyme CYP26A1 inhibitors.

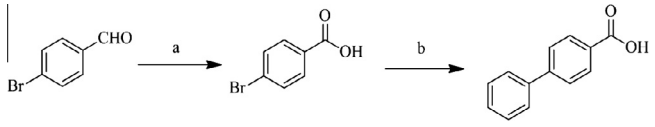

Scheme 1. Reagents and conditions: (a) 2 N NaOH, $KMnO_4$, 70 °C, 5 h.; (b) phenylboronic acid, K_2CO_3, $Pd[P(C_6H_5)_3]_4$, reflux, 5 h.

afforded yellow solid **5**. At last, the purified intermediate (compound **6**) was obtained by oxidation of the yellow solid compound **5** with potassium permanganate.[27]

The synthesis of key intermediate benzo[*d*]thiazole-2-carboxylic acid **10** was summarized in Scheme 3. The main chain compound **10** was synthesized from aniline, which was dissolved in diethyl oxalate and refluxed for 5 h to afford compound **7**. Subsequently, the oxygen atom of amide group was replaced by sulfur using Lawesson's Reagent to provide compound **8**.[28] Then, the compound **8** was hydrolyzed to corresponding aromatic acid **9** in the alkaline condition. Finally, the key intermediate **10** was successfully obtained via the cyclization reaction in the presence of potassium ferricyanide.[29]

Target compounds **15–29** were prepared as synthetic route outlined in Scheme 4. The side chains serine ester **11a–h** were synthesized from L-serine, the L-serine was dissolved in alcohol and refluxed with $SOCl_2$ for 6 h. Subsequently, the compounds **11a–h** were separately treated with the key intermediate (**2, 6, 10**) in the presence of condensing agent to give the required products **12 to 14a–e**.[30] Next, introduction of the imidazole groups, using

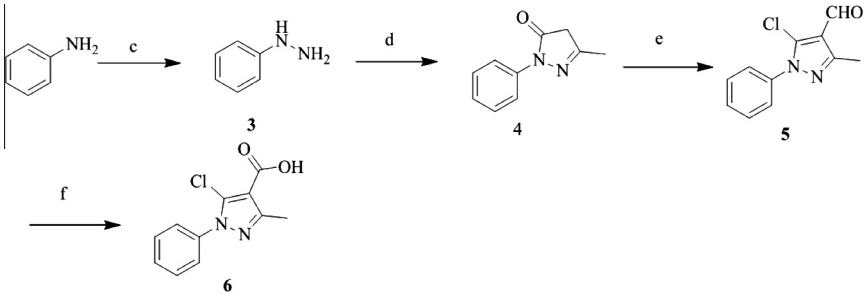

Scheme 2. Reagents and conditions: (c) $SnCl_2$, $NaNO_2$, HCl, 25 °C, 5 h; (d) ethyl acetoacetate, anhydrous ethanol, reflux, 7 h; (e) $POCl_3$, DMF, reflux, 2 h; (f) $KMnO_4$, H_2O, 90–95 °C, 4 h.

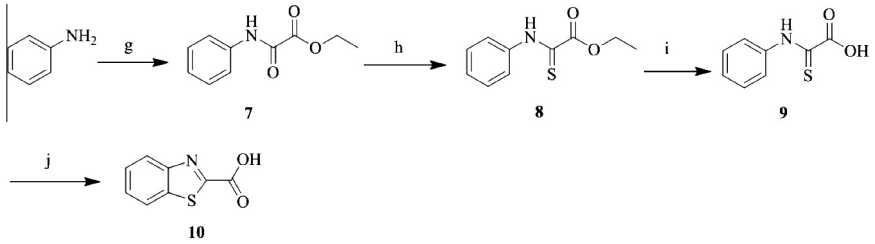

Scheme 3. Reagents and conditions: (g) diethyl oxalate, 150 °C, 5 h; (h) Lawesson's reagent, toluene, reflux, 7 h; (i) 2 N NaOH, 0–25 °C, 2 h; (j) $K_3[Fe(CN)_6]$, H_2O, 0–25°C, 4 h.

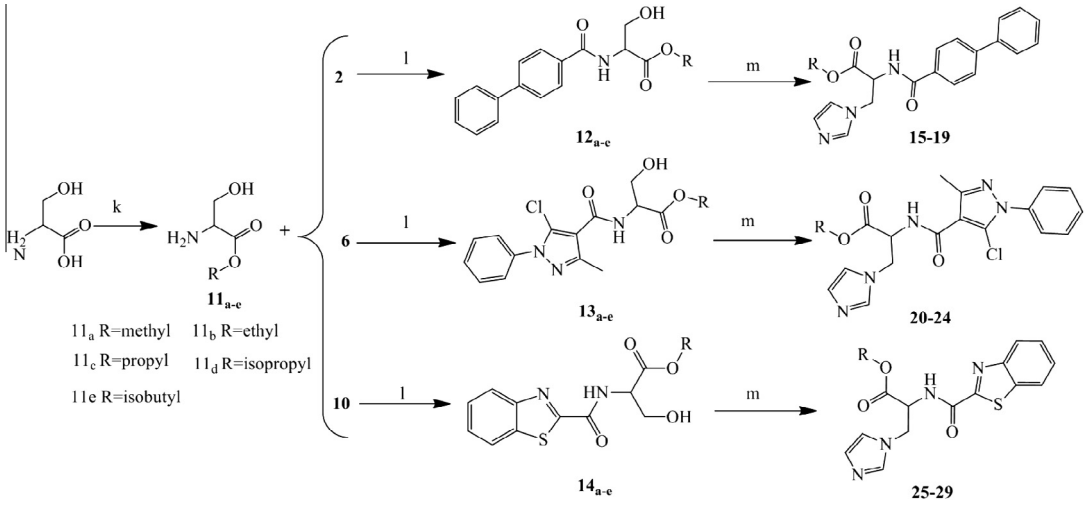

Scheme 4. Reagents and conditions: (k) alcohol reagent, $SOCl_2$, reflux, 24–48 h; (l) EDCI, HOBt, DIEA, reflux, 7 h; (m) CDI, imidazole, DMF, reflux, 7 h.

CDI/imidazole, gave the final products **15–29** following described methodology.[31]

2.3. CYP26A1 enzyme inhibition assay

All the newly synthesized amide imidazole derivatives were evaluated for their inhibitory activity toward CYP26A1 enzyme using a microsomal CYP26A1 inhibition assay as previously described.[13] The liarozole was used as control. The results were summarized in Table 1.

As illustrated in Table 1, all the tested compounds displayed CYP26A1 enzymatic activities with IC_{50} values ranging from 0.22 to 1.11 μM. Compared with liarozole (IC_{50} = 0.89 μM), most of the compounds showed moderate or higher potency, which suggested that the replacement of the main chain groups, imidazole group and side chain groups with different groups maintained the CYP26A1 inhibitory efficacy. Among them, compound **20** (IC_{50} = 0.22 μM) showed the highest activity, possibly due to the aryl pyrrole group forming much stronger interactions with the surrounding hydrophobic amino acids in the pocket A. In addition, the steric effects became more obvious when the main chain groups were fixed and the side chain groups were varied. With the increase of the length of the ester group fragment as the side chain groups, the inhibitory activities of those compounds showed obvious decline. The inhibitory activities of compound **15** (IC_{50} = 0.37 μM), **20** (IC_{50} = 0.22 μM) and **25** (IC_{50} = 0.41 μM) with methyl ester as the side chain group were significantly higher than the rest of compounds in the same group, suggesting that methyl ester as the side chain group was the optimal substituent at that position. Introduction of propyl ester and isobutyl ester groups led to a significant reduction in activity, such as the comparison of compound **15** (IC_{50} = 0.37 μM) and compound **17** (IC_{50} = 0.79 μM), compound **15** (IC_{50} = 0.37 μM) and compound **19** (IC_{50} = 0.97 μM). This can be explained that the small volume of a methyl group as the side chain group is possibly the best fit for pocket C of CYP26A1 metabolic enzyme. Moreover, it was worth noting that the compounds with an isopropyl ester group displayed higher potency than those with a propyl ester or an isobutyl ester side chain groups but lower potency than a methyl group. This is possibly due to the extra hydrophobic interactions from the branched methyl group in the isopropyl group, compensating the steric hindrance from the lengthening of the isopropyl group compared to a methyl group alone as the side chain group. The compensation is still not large enough, however. That is why

Table 1
IC_{50} values for the amide imidazole derivatives **15–29**

Compd	M	R	CYP26A1 IC_{50} (μM)
15	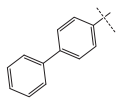	Methyl	0.37
16		Ethyl	0.65
17		Propyl	0.79
18		Isopropyl	0.54
19		Isobutyl	0.97
20	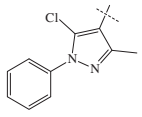	Methyl	0.22
21		Ethyl	0.60
22		Propyl	0.62
23		Isopropyl	0.46
24		Isobutyl	1.02
25	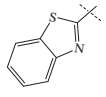	Methyl	0.41
26		Ethyl	0.74
27		Propyl	0.84
28		Isopropyl	0.63
29		Isobutyl	1.11
Liarozole			0.89

Note: M: the main chain groups. R: the side chain groups.

their activities are still lower than those with a methyl group as the side chain.

2.4. CYP26A1 binding model and pharmacophore matching model analysis

Previous studies showed that an imidazole or triazole group in RAMBAs for pocket B of CYP26A1 is possibly an essential moiety for their potent inhibition of CYP26A1 due to their ability to form a coordinate bond with the heme group of CYP26A1.[13–16] The underlying structural reasons for the high affinity of the amide imidazole derivatives were examined in silico by constructing a model of docked compounds **15**, **20**, and **25** in the CYP26A1 (shown in Fig. 5A and B) and a common feature pharmacophore matching model (shown in Fig. 6B).

In the docking model, compounds **15**, **20**, **25** occupied the substrate-binding site of the CYP26A1 enzyme, in which the imidazole group of those compounds formed a coordinate bond with the heme group of CYP26A1 (coordinate bond length 2.986 Å). The fact that an imidazole group in RAMBAs is more capable of interacting with the iron ion of the heme group than the cyclohexene structure of retinoic acid made them more competitive to the CYP26A1 enzyme, thus blocking the metabolism of retinoic acid (Fig. 6A). The main chain groups of all the compounds were surrounded by hydrophobic residues (Phe183, Phe260, Val331, Pro332, Phe335, Lys436 and Pro439), and the aromatic groups in the main chain groups formed hydrophobic interactions with the key residues Phe183, Val331, Pro332 and Lys436, respectively. That is why the amide imidazole derivatives with aromatic groups as their main chain groups have higher potency for CYP26A1 than retinoic acid with conjugate hydrophobic long chain moiety. The ester group on the side chain groups of derivatives fitted into pocket C of CYP26A1, in which the key residues of Trp73, Leu81 were close to the side chain groups. Visual inspection upon this pocket revealed that the methyl group is indeed the optimal substituent as the side chain group of RAMBAs (Fig. 5B). Any other groups larger than a methyl group would undoubtedly introduce steric hindrance, as demonstrated in the decline of inhibitory activities (Table 1). This can also help explain why the second generation RAMBAs are much better than the first generation because the latter have phenyl substituents as the side chain group, which would be definitely too large for pocket C and too much steric hindrance introduced.

In order to further evaluate the docking results, the molecular docking with the pharmacophore matching model was produced as described previously (Fig. 6B).[21] These results suggested that compounds **15**, **20**, **25** have very similar bioactive conformations compared to other RAMBAs, and they match the ligand-based pharmacophore model well. The aromatic groups of main chain moieties occupied three consecutive hydrophobic groups (H2, H3 and H4). The side chain groups matched hydrophobic group H1, and the imidazole group acted as a hydrogen bond acceptor (A) pointing to the center of the heme group.

2.5. In vitro cell growth inhibition and differentiation-inducing assay

All the newly synthesized amide imidazole derivatives were evaluated for their inhibitory and differentiation-inducing activities toward the CYP26A1 high expression *HL60* cells using the cell growth inhibition assay and cell differentiation-inducing assay as previously described.[32,33] Liarozole was used as control, and ATRA was used as the substrate. The results expressed as percentage of growth inhibition and percentage of differentiation-inducing activities are summarized in Table 2. The percentage of growth inhibition and the percentage of differentiation-inducing activities are the average of at least three independent experiments.

From the results in Table 2, it was observed that it was ATRA, rather than other compounds, can produce growth inhibition and differentiation-inducing activities of *HL60* cells. The percentage of inhibition and differentiation-inducing activities for *HL60* cells was 21.84 ± 2.6% and 28.04 ± 1.39% upon single administration of 0.1 μM ATRA, respectively. The percentage of inhibition and differentiation-inducing activities were moderately enhanced upon coadministration of ATRA with compounds **15–29**. Among these compounds, the growth inhibition and differentiation-inducing activities of compounds **15**, **18**, **20**, **21**,**25** and **28** were significantly higher than those of liarozole. Moreover, it was worth noting that compound **18** (percentage of growth inhibition activity = 54.58 ± 1.90%, percentage of differentiation-inducing activity = 53.91 ± 0.95%) with isopropyl ester side chain, and compound **20** (percentage of growth inhibition activity = 55.36 ± 2.04%, percentage of differentiation-inducing activity = 50.51 ± 1.28%) with methyl ester side chain displayed higher potency than other compounds in growth inhibition and differentiation-inducing activities. Also among those compounds, it was found that compounds **23** and **28** did not significantly inhibit the growth of *HL60* cells with obvious differentiation enhancement (compound **23**, percentage of differentiation-inducing activity = 51.85 ± 1.57%; compound **28**, percentage of differentiation-inducing activity = 50.85 ± 1.61%), which indicated that both compounds may have selectivity to inhibit CYP26A1 and then block ATRA metabolism.

2.6. Enzymatic selectivity assays

Over 90% of drug oxidation can be attributed to the following CYPs: 1A2 (4%), 2A6 (2%), 2C9(10%), 2C19 (2%), 2E1 (2%), 2D6 (30%), and 3A4 (50%). CYP3A4 and CYP2D6 are important metabolic enzymes in vivo.[34] To examine whether the compounds **20** and **23** with good CYP26A1 enzyme activity and cell activity are selective CYP26A1 inhibitors, the compounds were screened against the other 2 important metabolic enzymes CYP3A4 and CYP2D6 (Table 3). Compared with its high potency against CYP26A1, although compounds **20** and **23** also exhibited certain inhibitory activities against CYP3A4 and CYP2D6, it was observed that the compound **23** (CYP3A4, IC_{50} = 4.92 μM; CYP2D6, IC_{50} = 9.64 μM) with isopropyl ester groups showed higher selectivity than compound **20** (CYP3A4, IC_{50} = 1.17 μM; CYP2D6, IC_{50} = 5.56 μM) with methyl ester groups. The inhibitory potency of compound **23** toward CYP3A4, CYP2D6 were roughly 11-fold to 21-fold lower than that of CYP26A1. The possible reason is compounds **20** and **23** gradually reduced the selectivity of metabolic enzymes CYP3A4 and CYP2D6 with the extension of the side chain ester fragment.

The results above can be rationalized from an analysis of the crystal structures for the active sites of CYP2D6 (PDB ID code: 3TDA)[35] and CYP3A4 (PDB ID code: 4NY4).[36] They are shown in the Figure 7A and B. It was seen that the active sites of those two metabolic enzymes have two binding pockets, which are the channel that substrate into the active site and the chamber containing heme structure. However, they also have some distinct differences. The cavity in the active site of CYP2D6 is relatively narrow, while that of CYP3A4 is relatively large, rendering it able to oxidize a broad range of small and large molecular substrates. Such subtle difference makes CYP selectivity against CYP enzymes very challenging. Modifications of the compounds are required to try to improve CYP26A1 selectivity, which will be the subject of further research.

Further binding model analyses of compound **23** with better CYP26A1 selectivity revealed that compound **23** has a reasonable binding mode (Fig. 8). The docking model demonstrated that the

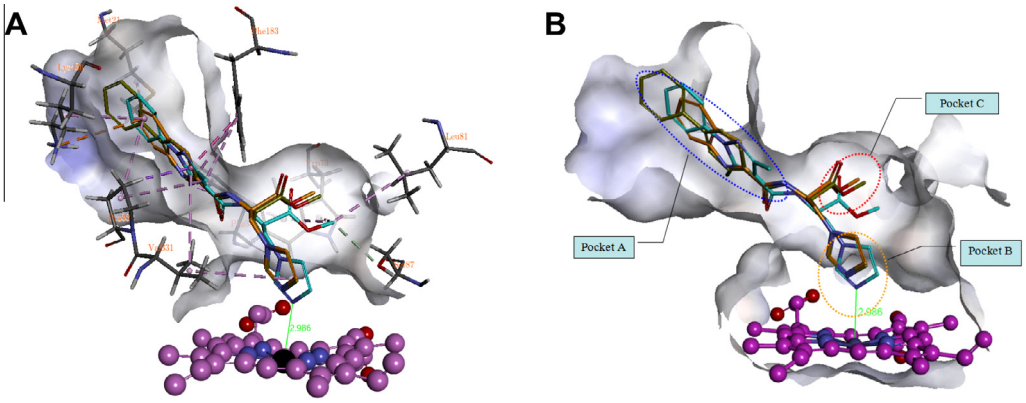

Figure 5. (A) Docked conformation of compounds **15**, **20**, and **25** showing important interactions with the binding site of CYP26A1. Only the interacting amino acid residues are shown in sticks. Hydrophobic interactions are shown as pink dotted lines. (B) Surface representation of CYP26A1 with compounds **15**, **20**, **25** into its binding site.

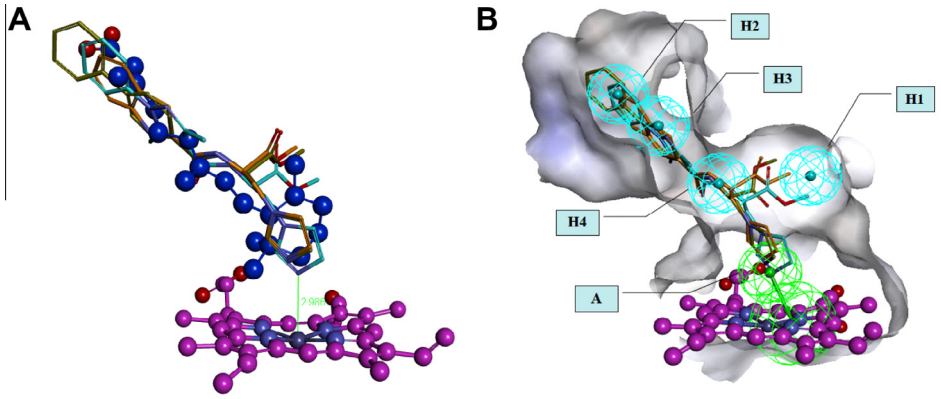

Figure 6. (A) Overlay of the conformations of reference compound (retinoic acid) obtained from the homology modeling of CYP26A1 structure (in blue) and present docking study. (B) The common feature pharmacophore model matching compounds **15**, **20**, and **25**.

Table 2
Growth inhibitory and differentiation-inducing activities of amide imidazole derivatives in combination with ATRA in *HL60* cells

Compd	Percentage of growth inhibition activities (%)			Percentage of differentiation-inducing activities (%)		
	0.1 μM ATRA	10 μM inhibitor	10 μM inhibitor + 0.1 μM ATRA	0.1 μM ATRA	10 μM inhibitor	10 μM inhibitor + 0.1 μM ATRA
ATRA	21.84 ± 2.66			28.04 ± 1.39		
15		9.64 ± 0.15	51.38 ± 1.84		0	47.69 ± 1.08
16		7.61 ± 1.08	48.19 ± 3.06		0	45.64 ± 1.30
17		5.04 ± 1.49	42.92 ± 3.06		0	44.78 ± 2.57
18		6.58 ± 2.91	54.58 ± 1.90		0	53.91 ± 0.95
19		8.99 ± 2.87	46.55 ± 1.90		0	39.87 ± 0.51
20		10.86 ± 0.98	55.36 ± 2.04		0	50.51 ± 1.28
21		7.25 ± 1.32	52.17 ± 2.64		0	46.44 ± 0.72
22		6.59 ± 2.10	45.58 ± 2.85		0	43.83 ± 1.62
23		4.98 ± 2.53	44.79 ± 2.92		0	51.85 ± 1.57
24		8.24 ± 0.73	43.54 ± 1.57		0	40.79 ± 0.48
25		8.64 ± 0.34	50.36 ± 1.26		0	49.11 ± 1.73
26		6.66 ± 1.91	45.40 ± 2.26		0	48.31 ± 0.86
27		7.64 ± 0.52	47.83 ± 1.31		0	42.62 ± 1.31
28		5.04 ± 1.49	46.36 ± 0.93		0	50.85 ± 1.61
29		9.49 ± 3.16	43.33 ± 3.06		0	38.62 ± 1.01
Liarozole		16.44 ± 1.74	48.37 ± 1.07		0	45.55 ± 2.94

Table 3
CYP IC_{50} (μM) profile of compounds **20** and **23** when compared with liarozole

Compd	CYP3A4 IC_{50} (μM)	CYP2D6 IC_{50} (μM)	CYP26A1 IC_{50} (μM)
20	1.17	5.56	0.22
23	4.92	9.64	0.46
Liarozole	0.69	4.76	0.89

arylpyrrole group in the main chain was located in the hydrophobic pocket A, forming Pi–cation interactions with the positively charged amino acid residue Lys436, Pi–sigma interactions with the hydrophobic amino acid residue Pro332, and Pi–Pi interactions with the hydrophobic amino acid residue Phe183. The imidazole group occupied pocket B, and the charge–charge interactions were formed between the basic nitrogen atom of the group and the heme group at the bottom of pocket B. Moreover, the docking

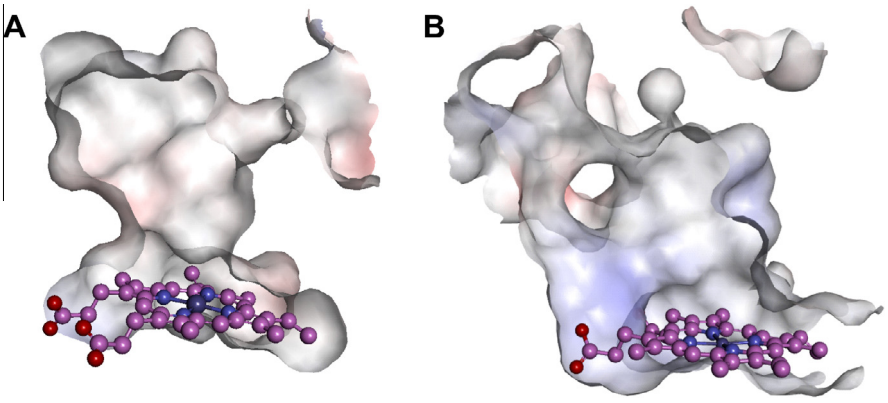

Figure 7. (A) The active chamber of metabolic enzyme CYP2D6. (B) The active chamber of metabolic enzyme CYP3A4.

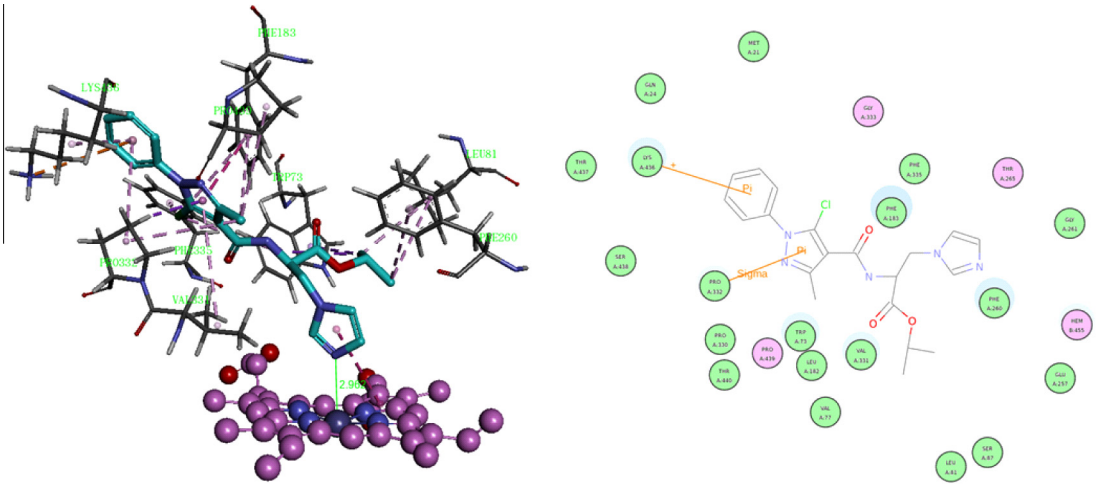

Figure 8. Binding model of compound **23** with CYP26A1.

model of compound **23** also demonstrated that the alkyl-sigma and Pi-alkyl hydrophobic interactions were formed between the side chain groups and the surrounding amino acid residues Leu81, Phe260.

2.7. Determination of metabolic profile of ATRA concentration with compound 20 or 23 by HPLC

In order to examine the effect on cellular metabolism of ATRA with compound **20** or **23**, two groups were used for determination of metabolic profile of ATRA concentration by HPLC: an ATRA (10 μM) single administration group in the presence of *HL60* cells (106 cells) and an ATRA (10 μM) and compound **20** or **23** (5 μM) coadministration group in the presence of *HL60* cells (106 cells). The concentrations of ATRA were determined after 0 h, 24 h, 48 h, 72 h, 96 h of addition of ATRA alone or with compounds **20** and **23**.

Table 4
Concentration and cyclic proportion of ATRA in different groups

Time (h)	ATRA	Compound **20** + ATRA	Compound **23** + ATRA
0	10	10	10
24	7.19	9.30	9.22
48	4.95	7.45	7.87
72	3.60	5.67	6.06
96	1.21	3.51	4.41

As illustrated in Table 4, with the addition of compound **20** or **23**, the concentrations of ATRA were reduced to 3.51 μm/L and 4.41 μm/L at 96 h, compared with the ATRA single administration group 1.21 μm/L. These data suggested that compounds **20** and **23** slowed down the ATRA metabolism by inhibiting CYP26A1 and other CYP enzymes.

3. Conclusions

RAMBAs of CYP26A1 are an important class of potential drugs to treat various cancers, especially APL. The first generation of RAMBAs has severe side effects due to its lack of CYP26 isoform specificity. The second generation of RAMBAs has dramatically reduced their side effects and increased their efficacy compared to their first generation counterparts. However, there is still much room for improvement in searching for new generations of RAMBAs. In this study, based on the homology model of CYP26A1, the common feature pharmacophore model, the molecular superimposition model as well as the SAR model we previously described,[21] a series of novel amide imidazole derivatives were designed using fragment-based drug discovery technology. Then those compounds were synthesized and evaluated using biochemical and cell-based assays for their activities against CYP26A1. Furthermore, *HL60* cell lines were used to evaluate their growth inhibition and differentiation-inducing activities. The results showed that most compounds displayed moderate or strong potency in growth inhibition and differentiation-inducing

activities in the cell lines. The analysis of the SAR indicated that those compounds with aryl pyrrole group as the main chain group were more active than those with other substituents. Furthermore, the introduction of a methyl ester or isopropyl ester groups as the side chain led to a big increase in the inhibitory activity. It was ascribed to the fact that a methyl or isopropyl group is able to fit pocket C better, avoiding steric hindrance that would exist for larger groups such as ethyl, propyl and isobutyl groups. Based on the experimental and computational results, compounds **20** and **23** were determined as promising CYP26A1 inhibitors. Further optimization on these compounds is underway.

4. Methods

4.1. Experimental

Commercial reagents and solvents were used without additional purification. The reaction progression was determined by thin layer chromatography (TLC) on Silica Gel 60 F254 plates (Jiangyou, Yantai). Column chromatography was run on silica gel (200–300 mesh) from Qingdao Ocean Chemicals (Qingdao, Shandong, China). The mass spectra (MS) were taken in ESI mode on an Agilent 1200 LC–MS (Agilent, Palo Alto, CA, USA). All melting points were determined on a BüCHI Melting Point B-540 melting point apparatus (Büchi Labortechnik, Flawil, Switzerland) and were not corrected. Proton nuclear magnetic resonance (^{1}H NMR) spectra were recorded on a Bruker DPX 300, 300 MHz spectrometer (Bruker Bioscience, Billerica, MA, USA) with TMS as an internal standard. The chemical shifts (d) were reported in ppm relative to internal tetramethylsilane. Peak multiplicities were expressed as follows: s, singlet; d, doublet; t, triplet; q, quartet; dd, doublet of doublet; dt, doublet of triplet; td, triplet of doublet; ddd, doublet of doublet of doublet; m, multiplet; br s, broad.

4.1.1. 4-Bromobenzoic acid (1)

Potassium permanganate (12 mmol) was added to 4-bromobenzaldehyde (10 mmol) in 20 mL of 2 N sodium hydroxide solution. After stirring for 4 h at 70 °C, the reaction mixture was filtered, adjusted to pH 1. A lot of white solid precipitation was filtered and dried in vacuo at 40 °C for 24 h to give a white solid (16.6 g, yield: 92.2%).

4.1.2. [1,1′-Biphenyl]-4-carboxylic acid (2)

In a 100 mL flask, phenylboronic acid (1.68 g, 12 mmol), K_2CO_3 (3.31 g, 24.0 mmol), $Pd[P(C_6H_5)_3]_4$ (0.2 g) and compound **1** (2 g,10 mmol) were dissolved into the mixed solution of dioxane/water (30/5 mL). Then the mixture was heated to 80–85 °C and was maintained at this temperature for 5 h. The reaction mixture was filtered, and the filtrate was adjusted to pH 2–3 with 2 N hydrochloric acid solution. A lot of white solid precipitation was filtered and dried in vacuo at 40 °C for 24 h to give a white solid (1.75 g, yield: 88.6%).

4.1.3. Phenylhydrazine hydrochloride (3)

In 100 mL round bottom flask, aniline (3.07 g, 33 mmol) was added to concentrated hydrochloric acid (20 mL). While being stirred at 0 °C, the aqueous solution of sodium nitrite (3.38 g, 49 mmol) was dropped slowly into the mixture, and the mixture was stirred for 30 min. Then hydrochloric acid solution of stannous chloride (3.07 g, 99 mmol) was dropped slowly into the mixture, and the mixture was stirred at room temperature for 5 h. The reaction process was monitored by TLC. After the completion of reaction, the product was filtered and dried in vacuo at 40 °C for 24 h to give a gray solid (4.37 g, yield: 92.2%).

4.1.4. 3-Methyl-1-phenyl-1*H*-pyrazol-5(4*H*)-one (4)

A stirred solution of phenylhydrazine hydrochloride(21.6 g, 200 mmol) in anhydrous ethanol (30 mL) was added with ethyl acetoacetate (26.0 g, 200 mmol), and the resulting reaction mixture was heated to 75 °C for 7 h, then the anhydrous ethanol was removed under reduced pressure, final the yellow solid was obtained (29.3 g, yield 85.0%). Mp: 128.0–130.3 °C; ESI-MS m/z: 175.1 $[M+H]^+$; 197.1 $[M+Na]^+$; 172.9 $[M-H]^-$.

4.1.5. 5-Chloro-3-methyl-1-phenyl-1*H*-pyrazole-4-carbaldehyde (5)

Phosphorus oxychloride (64 mL, 700 mmol) was added dropwise at a rate to a cold solution (0–5 °C) of *N*,*N*-dimethylformamide (23 ml, 300 mmol). After 30 min, 3-methyl-1-phenyl-1*H*-pyrazol-5(4*H*) one **6** (17.48 g, 100 mmol) was added. The resulting mixture was allowed to heat to 100 °C for 2 h. The reaction mixture was poured slowly into the mixed solution of cold water (600 mL), a lot of precipitated solid was filtered and dried in vacuo at 40 °C for 24 h to give a light yellow solid (19.0 g, yield: 86.4%); mp: 139.0–140.8 °C; ESI-MS m/z: 221.1 $[M+H]^+$; 243.1 $[M+Na]^+$.

4.1.6. 5-Chloro-3-methyl-1-phenyl-1*H*-pyrazole-4-carbaldehyde (6)

5-Chloro-3-methyl-1-phenyl-1*H*-pyrazole-4-carbaldehyde **5** (16.85 g, 76.4 mmol) and potassium permanganate was added to the solution of water (300 mL) and heated to 90–95 °C for 4 h. The reaction mixture was filtered, adjusted to pH 1. A lot of precipitated white solid was filtered and dried in vacuo at 40 °C for 24 h to give a white solid (16.6 g, yield: 92.2%); mp: 232.1–234.7 °C; ^{1}H NMR (DMSO-d_6, 300 MHz) δ(ppm): 2.41 (s, 3H), 7.56 (s, 5H), 12.88 (s, 1H); ESI-MS m/z: 237.1 $[M+H]^+$; 259.1 $[M+Na]^+$.

4.1.7. Ethyl 2-oxo-2-(phenylamino)acetate (7)

A stirred solution of diethyl oxalate (30 mL, 221.92 mmol) was added with phenylamine (5 g, 53.8 mmol), The mixture was then heated to 150 °C for 5 h. The reaction mixture was allowed to cool and poured into 100 ml of petroleum ether. A lot of precipitated white solid was filtered and dried in vacuo at 40 °C for 24 h to give a white solid (8.52 g, yield: 82.1%).

4.1.8. Ethyl 2-(phenylamino)-2-thioxoacetate (8)

Lawesson's reagent (2.1 g, 5.2 mmol) was added to a solution of ethyl 2-oxo-2-(phenylamino) acetate **7** (2 g, 10.4 mmol) in toluene (30 mL), the reaction mixture was stirred at 75 °C for 7 h. The crude mixture was concentrated under reduced pressure and purified by column chromatography (petroleum ether/ethyl acetate 10:1) to give compound **8** (1.59 g, 73.6%) as red crystals. ESI-MS m/z: 210.1 $[M+H]^+$; 232.1 $[M+Na]^+$.

4.1.9. Benzo[*d*]thiazole-2-carboxylic acid (10)

The solution of 2 N sodium hydroxide 30 mL was added to a solution of ethyl 2-(phenylamino)-2-thioxoacetate **8** (1.5 g, 7.2 mmol) in dichloromethane (10 mL). The reaction was stirred at room temperature for 2 h, the reaction process was monitored by TLC. After the completion of reaction, the dichloromethane was removed under reduced pressure.

The potassium ferricyanide (7.08 g, 21.6 mmol) was dissolved in the solution of water (21 mL), and the mixture was added to the above reaction solution, the reaction was stirred at room temperature for 4 h. The above reaction solution was adjusted to pH 2–3 with 2 N hydrochloric acid solution. A lot of white solid precipitation was filtered and dried in vacuo at 40 °C for 24 h to give a white solid **10** (0.93 g, yield: 72.1%); ESI-MS m/z:180.0 $[M+H]^+$; 202.0 $[M+Na]^+$; 177.8 $[M-H]^-$.

4.2. General procedure for the synthesis of L-serine ester (11_{a-e})

Thionylchloride (1 equiv) was added dropwise to the alcohol at a rate to maintain the temperature below 5 °C. After 30 min, L-serine $\mathbf{9_a–9_l}$ (3 equiv) was added in the reaction under reflux for 24–48 h, respectively. Then the alcohol was removed under reduced pressure, final white solid was obtained.

4.3. General procedure for the synthesis of compounds (12_{a-e}, 13_{a-e}, 14_{a-e})

EDCI (1.1 equiv) and HOBt (1.1 equiv) were added to a solution of appropriate organic acids 2, 6 and 10 (1 equiv) in anhydrous DMF, respectively. The mixture was stirred at room temperature for 2 h, then L-serine ester **11a–e** (1.1 equiv) and DIEA (4 equiv) were added, and the mixture was heated at 75 °C for 7 h. The reaction mixture was poured into ice water, filtered and produced a white solid.

4.4. General procedure for the synthesis of compounds (15–29)

To solution of compounds **12a–e, 13a–e, 14a–e** (1 equiv) in anhydrous CH_3CN was added imidazole (2 equiv) and CDI (3 equiv). The mixture was then heated under reflux for 7 h. The reaction mixture was allowed to cool and then extracted with EtOAc and H_2O. The organic layer was dried ($MgSO_4$) filtered and reduced in vacuo. The product was purified by flash column chromatography.

4.4.1. Methyl 2-([1,1′-biphenyl]-4-ylcarboxamido)-3-(1*H*-imidazol-1-yl)propanoate (15)

Light white solid; yield: 53.2%; mp: 131.9–135.5 °C. ^{1}H NMR (400 MHz, DMSO-d_6) δ(ppm): 9.10 (d, J = 8.0 Hz, 1H), 7.93 (d, J = 8.3 Hz, 2H), 7.80 (d, J = 8.3 Hz, 2H), 7.74 (d, J = 7.4 Hz, 2H), 7.70 (s, 1H), 7.50 (t, J = 7.5 Hz, 2H), 7.42 (d, J = 7.3 Hz, 1H), 7.24 (s, 1H), 6.89 (s, 1H), 4.96–4.83 (m, 1H), 4.51 (d, J = 24.0 Hz, 2H), 3.71 (s, 3H). ^{13}C NMR (150 MHz, DMSO-d_6) δ(ppm): 170.62(C=O), 166.69 (C=O), 143.74 (ArC), 139.54 (ArC), 138.30 (ArCH), 132.59 (ArC), 129.70 (ArCH), 129.50 (2×ArCH), 128.61 (ArCH), 128.52 (2×ArCH), 127.38 (2×ArCH), 127.10 (2×ArCH), 120.41 (ArCH), 54.14 (CH_3), 52.78 (CH), 46.28 (CH_2). ESI-MS m/z: 350.0 $[M+H]^+$; 372.1 $[M+Na]^+$; 348.1 $[M-H]^-$.

4.4.2. Ethyl 2-([1,1′-biphenyl]-4-ylcarboxamido)-3-(1*H*-imidazol-1-yl)propanoate (16)

Light white solid; yield: 61.4%; mp: 137.4–141.1 °C. ^{1}H NMR (400 MHz, DMSO-d_6) δ(ppm): 9.04 (d, J = 7.9 Hz, 1H), 7.91 (d, J = 8.3 Hz, 2H), 7.80 (d, J = 8.3 Hz, 2H), 7.74 (d, J = 7.4 Hz, 2H), 7.67 (s, 1H), 7.50 (t, J = 7.5 Hz, 2H), 7.42 (t, J = 7.3 Hz, 1H), 7.24 (s, 1H), 6.87 (s, 1H), 4.84 (m, 1H), 4.48 (d, J = 23.9 Hz, 2H), 4.16 (q, J = 7.1 Hz, 2H), 1.19 (t, J = 7.1 Hz, 3H). ^{13}C NMR (150 MHz, DMSO-d_6) δ(ppm): 169.64 (C=O), 166.74 (C=O), 143.67 (ArC), 139.56 (ArC), 138.31 (ArCH), 132.75 (ArC), 129.50 (2×ArCH), 128.82 (ArCH), 128.59 (ArCH), 128.47 (2×ArCH), 127.37 (2×ArCH), 127.10 (2×ArCH), 120.35 (ArCH), 69.11 (CH_2), 54.38 (CH), 46.23 (CH_2), 21.95 (CH_3). ESI-MS m/z: 364.2 $[M+H]^+$; 386.3 $[M+Na]^+$; 362.2 $[M-H]^-$.

4.4.3. Propyl 2-([1,1′-biphenyl]-4-ylcarboxamido)-3-(1*H*-imidazol-1-yl)propanoate (17)

Light white solid; yield: 57.1%; mp: 142.1–146.2 °C. ^{1}H NMR (400 MHz, DMSO-d_6) δ(ppm): 9.04 (d, J = 8.0 Hz, 1H), 7.90 (d, J = 8.4 Hz, 2H), 7.81–7.77 (m, 2H), 7.75–7.71 (m, 2H), 7.70 (s, 1H), 7.50 (t, J = 7.5 Hz, 2H), 7.43 (d, J = 7.3 Hz, 1H), 7.24 (s, 1H), 6.89 (s, 1H), 4.85 (m, 1H), 4.57–4.38 (d, J = 48 Hz, 2H), 4.07 (t, J = 8.7 Hz, 2H), 1.59 (m, J = 20.8 Hz, 2H), 0.87 (t, J = 7.4 Hz, 3H). ^{13}C NMR (150 MHz, DMSO-d_6) δ(ppm): 170.15 (C=O), 166.74 (C=O), 143.69 (ArC), 139.54 (ArC), 138.24 (ArCH), 132.68 (ArC), 129.50 (2×ArCH), 128.60 (ArCH), 128.47 (2×ArCH), 127.81 (ArCH), 127.37 (2×ArCH), 127.10 (2×ArCH), 120.41 (ArCH), 66.88 (CH_2), 54.25 (CH), 46.25 (CH_2), 21.92 (CH_2), 10.66 (CH_3). ESI-MS m/z: 378.2 $[M+H]^+$; 400.3 $[M+Na]^+$; 376.2 $[M-H]^-$.

4.4.4. Isopropyl 2-([1,1′-biphenyl]-4-ylcarboxamido)-3-(1*H*-imidazol-1-yl)propanoate (18)

Light white solid; yield: 55.9%; mp: 144.9–149.7 °C. 1H NMR (400 MHz, DMSO-d_6) δ(ppm): δ 9.02 (d, J = 7.9 Hz, 1H), 7.90 (d, J = 8.3 Hz, 2H), 7.80 (d, J = 8.3 Hz, 2H), 7.74 (d, J = 7.3 Hz, 2H), 7.65 (s, 1H), 7.50 (t, J = 7.5 Hz, 2H), 7.42 (t, J = 7.3 Hz, 1H), 7.24 (s, 1H), 6.87 (s, 1H), 4.96 (m, J = 18.7 Hz, 1H), 4.85–4.71 (m, 1H), 4.47 (d, J = 35.3 Hz, 2H), 1.20 (t, J = 5.9 Hz, 6H). ^{13}C NMR (150 MHz, DMSO-d_6) δ(ppm): 170.12 (C=O), 166.70 (C=O), 143.70 (ArC), 139.54 (ArC), 138.30 (ArCH), 132.66 (ArC), 129.51 (2×ArCH), 128.76 (ArCH), 128.61 (ArCH), 128.49 (2×ArCH), 127.38 (2×ArCH), 127.10 (2×ArCH), 120.37 (ArCH), 61.53 (CH), 54.24 (CH), 46.25 (CH_2), 21.92 (CH_2), 14.48 (2×CH_3). ESI-MS m/z: 378.2 $[M+H]^+$; 400.3 $[M+Na]^+$; 376.2 $[M-H]^-$.

4.4.5. Isobutyl 2-([1,1′-biphenyl]-4-ylcarboxamido)-3-(1*H*-imidazol-1-yl)propanoate (19)

Light white solid; yield: 55.9%; mp: 147.3–153.5 °C. ^{1}H NMR (400 MHz, DMSO-d_6) δ(ppm): 9.04 (d, J = 8.0 Hz, 1H), 7.89 (d, J = 8.4 Hz, 2H), 7.82–7.70 (m, 4H), 7.46 (m, 7.3 Hz, 3H), 7.23 (s, 1H), 6.86 (s, 1H), 4.84 (m, 1H), 4.50 (d, J = 45.4 Hz, 2H), 3.91 (d, J = 6.1 Hz, 2H), 1.87 (m, 1H), 0.87 (d, J = 6.7 Hz, 7H). ^{13}C NMR (150 MHz, DMSO-d_6) δ(ppm): 170.09 (C=O), 166.77 (C=O), 143.67 (ArC), 139.53 (ArC), 138.28 (ArCH), 132.71(ArC), 129.51 (2×ArCH), 128.78 (ArCH), 128.61 (ArCH), 128.44 (2×ArCH), 127.37 (2×ArCH), 127.10 (2×ArCH), 120.33 (ArCH), 71.11 (CH_2), 54.27 (CH), 46.15 (CH_2), 27.70 (CH), 19.21 (2×CH_3). ESI-MS m/z: 392.2 $[M+H]^+$; 414.3 $[M+Na]^+$; 390.2 $[M-H]^-$.

4.4.6. Methyl 2-(5-chloro-3-methyl-1-phenyl-1*H*-pyrazole-4-carboxamido)-3-(1*H*-imidazol-1-yl)propanoate (20)

Light white solid; yield: 59.5%; mp: 141.3–145.8 °C. ^{1}H NMR (400 MHz, DMSO-d_6) δ(ppm): 8.46–8.44 (d, J = 8.0 Hz, 1H), 7.62 (s, 1H), 7.60–7.52 (m, 5H), 7.21 (s, 1H), 6.88 (s, 1H), 4.88–4.82 (m, 1H), 4.53–4.34 (d, J = 76 Hz, 2H), 3.33 (s, 3H), 2.22 (s, 3H). ^{13}C NMR (150 MHz, DMSO-d_6) δ(ppm): 170.30 (C=O), 162.15 (C=O), 149.27 (ArC), 138.33 (ArCH), 137.61(ArC), 129.81 (2×ArCH), 129.43 (ArC), 128.83 (ArCH), 126.94 (ArCH), 125.81 (2×ArCH), 120.28 (ArCH), 114.66 (ArC), 71.11 (CH_3), 52.81 (CH), 46.25 (CH_2), 13.62 (CH_3). ESI-MS m/z: 388.1 $[M+H]^+$; 410.3 $[M+Na]^+$; 386.2 $[M-H]^-$.

4.4.7. Ethyl 2-(5-chloro-3-methyl-1-phenyl-1*H*-pyrazole-4-carboxamido)-3-(1*H*-imidazol-1-yl)propanoate (21)

Light white solid; yield: 53.2%; mp: 144.9–148.5 °C. ^{1}H NMR (400 MHz, DMSO-d_6) δ(ppm): 8.48–8.46 (d, J = 8 Hz,1H), 7.66 (s, 1H), 7.58–7.52 (m, 5H), 7.23 (s, 1H), 6.90 (s, 1H), 4.84–4.79 (m, 1H), 4.53–4.35 (d, J = 72 Hz, 2H), 4.17 (q, J = 8 Hz, 2H), 2.23 (s, 3H), 1.22 (t, J = 8 Hz,3H). 13C NMR (150 MHz, DMSO-d_6) δ(ppm): 169.79 (C=O), 162.10 (C=O), 149.19 (ArC), 138.30 (ArCH), 137.64 (ArC), 129.80 (2×ArCH), 129.40 (ArC), 128.66 (ArCH), 126.87 (ArCH), 125.79 (2×ArCH), 120.34 (ArCH), 114.83 (ArC), 61.58 (CH_2), 53.83 (CH), 46.28 (CH_2), 14.45 (CH_3), 13.59 (CH_3). ESI-MS m/z: 402.1 $[M+H]^+$; 424.3 $[M+Na]^+$; 400.2 $[M-H]^-$.

4.4.8. Propyl 2-(5-chloro-3-methyl-1-phenyl-1*H*-pyrazole-4-carboxamido)-3-(1*H*-imidazol-1-yl)propanoate (22)

Light white solid; yield: 63.7%; mp: 146.3–151.4 °C. ^{1}H NMR (400 MHz, DMSO-d_6) δ(ppm): 8.49–8.47 (d, J = 8.0 Hz, 1H), 7.69 (s, 1H), 7.60–7.53 (m, 5H), 7.25 (s, 1H), 6.92 (s, 1H), 4.86–4.81 (m, 1H), 4.54–4.36 (d, J = 72 Hz, 2H), 4.10–4.06 (t, J = 8 Hz, 2H),

2.23 (s, 3H), 1.64–1.57 (m, 2H), 0.92–0.88 (t, J = 8 Hz, 3H). ^{13}C NMR (150 MHz, DMSO-d_6) δ(ppm): 169.83 (C=O), 162.10 (C=O), 149.20 (ArC), 138.25 (ArCH), 137.63 (ArC), 129.81 (2×ArCH), 129.41 (ArC), 128.44 (ArCH), 126.87 (ArCH), 125.79 (2×ArCH), 120.39 (ArCH), 114.79 (ArC), 66.98 (CH_2), 53.80 (CH), 46.32 (CH_2), 21.93 (CH_2), 13.58 (CH_3), 10.71 (CH_3). ESI-MS m/z: 416.1 $[M+H]^+$; 438.3 $[M+Na]^+$; 414.2 $[M-H]^-$.

4.4.9. Isopropyl 2-(5-chloro-3-methyl-1-phenyl-1*H*-pyrazole-4-carboxamido)-3-(1*H*-imidazol-1-yl)propanoate (23)

Light white solid; yield: 61.8%; mp: 153.4–158.5 °C. ^{1}H NMR (400 MHz, DMSO-d_6) δ(ppm): 8.48–8.47(d, J = 4 Hz, 1H), 7.62(s, 1H), 7.58–7.52(m, 5H), 7.22(s, 1H), 6.88 (s, 1H), 5.00–4.94 (m, 1H), 4.78–4.72 (m, 1H), 4.50–4.34 (d, J = 64 Hz, 2H), 2.23 (s, 3H), 1.22–1.2 (q, J = 4 Hz,6H). ^{13}C NMR (150 MHz, DMSO-d_6) δ (ppm): 169.27 (C=O), 162.06 (C=O), 149.14 (ArC), 138.33 (ArCH), 137.64 (ArC), 129.80 (2×ArCH), 129.39 (ArC), 128.80 (ArCH), 126.83 (ArCH), 125.78 (2×ArCH), 120.28 (ArCH), 114.92 (ArC), 69.18 (CH), 53.99 (CH), 46.19 (CH_2), 21.94 (2×CH_3), 13.56 (CH_3). ESI-MS m/z: 416.1 $[M+H]^+$; 438.3 $[M+Na]^+$; 414.2 $[M-H]^-$.

4.4.10. Isobutyl 2-(5-chloro-3-methyl-1-phenyl-1*H*-pyrazole-4-carboxamido)-3-(1*H*-imidazol-1-yl)propanoate (24)

Light white solid; yield: 57.4%; mp: 151.6–156.7 °C. ^{1}H NMR (400 MHz, DMSO-d_6) δ(ppm): 8.49–8.47 (d, J = 8 Hz,1H), 7.77 (s, 1H), 7.60–7.52 (m, 5H), 7.28 (s, 1H), 6.96 (s, 1H), 4.89–4.84 (m, 1H), 4.56–4.39 (d, J = 68 Hz, 2H), 3.93–3.91 (d, J = 8 Hz, 2H), 2.22 (s, 3H), 1.93–1.86 (m, 1H), 0.91–0.89 (d, J = 8 Hz, 6H). ^{13}C NMR (150 MHz, DMSO-d_6) δ(ppm): 169.75 (C=O), 162.10 (C=O), 149.22 (ArC), 138.17 (ArCH), 137.62 (ArC), 129.81 (2×ArCH), 129.41 (ArC), 128.04 (ArCH), 126.88 (ArCH), 125.78 (2×ArCH), 120.51 (ArCH), 114.74 (ArC), 71.26 (CH_2), 53.72 (CH), 46.41 (CH_2), 27.73 (CH), 19.27 (2×CH_3), 13.59 (CH_3). ESI-MS m/z: 430.2 $[M+H]^+$; 452.3 $[M+Na]^+$; 428.2 $[M-H]^-$.

4.4.11. Methyl 2-(benzo[*d*]thiazole-2-carboxamido)-3-(1*H*-imidazol-1-yl)propanoate (25)

Light white solid; yield: 59.1%; mp: 141.6–146.7 °C. ^{1}H NMR (400 MHz, DMSO-d_6) δ(ppm): 9.68–9.65 (d, J = 12 Hz, 1H), 8.25–8.23 (d, J = 8 Hz, 1H), 8.19–8.17 (d, J = 8 Hz,1H), 7.68–7.59 (m, 3H), 7.20 (s, 1H), 6.83 (s, 1H), 5.02–4.96 (m, 1H), 4.62–4.47 (d, J = 60 Hz, 2H), 3.72 (s, 3H). ^{13}C NMR (150 MHz, DMSO-d_6) δ (ppm): 169.77 (C=O), 163.68 (C=O), 160.20 (ArC), 153.03 (ArC), 138.26 (ArCH), 136.60 (ArC), 128.85 (ArCH), 127.77 (ArC), 127.65 (ArCH), 124.57 (ArCH), 123.60 (ArCH), 120.27 (ArCH), 53.87 (CH_3), 53.00 (CH), 46.04 (CH_2). ESI-MS m/z: 331.2 $[M+H]^+$; 453.3 $[M+Na]^+$; 429.2 $[M-H]^-$.

4.4.12. Ethyl 2-(benzo[*d*]thiazole-2-carboxamido)-3-(1*H*-imidazol-1-yl)propanoate (26)

Light white solid; yield: 62.6%; mp: 137.8–142.2 °C. ^{1}H NMR (400 MHz, DMSO-d_6) δ(ppm): 9.67–9.64 (d, J = 12 Hz, 1H), 8.25–8.23 (d, J = 8 Hz, 1H), 8.19–8.17 (d, J = 8 Hz, 1H), 7.76 (s, 1H), 7.68–7.59 (m, 2H), 7.26 (s, 1H), 6.90 (s, 1H), 4.99–4.94 (m, 1H), 4.63–4.48 (d, J = 60 Hz, 2H), 4.20–4.15 (q, J = 12 Hz, 2H), 1.22–1.18 (t, J = 4 Hz, 3H). ^{13}C NMR (150 MHz, DMSO-d_6) δ(ppm): 169.21 (C=O), 163.68 (C=O), 160.23 (ArC), 153.04 (ArC), 138.14 (ArCH), 136.59 (ArC), 128.08 (ArCH), 127.77 (ArC), 127.65 (ArCH), 124.57 (ArCH), 123.60 (ArCH), 120.55 (ArCH), 61.84 (CH_2), 53.92 (CH), 46.28 (CH_2), 14.45 (CH_3). ESI-MS m/z: 345.2 $[M+H]^+$; 367.3 $[M+Na]^+$; 343.2 $[M-H]^-$.

4.4.13. Propyl 2-(benzo[*d*]thiazole-2-carboxamido)-3-(1*H*-imidazol-1-yl)propanoate (27)

Light white solid; yield: 62.6%; mp: 147.5–152.6 °C. ^{1}H NMR (400 MHz, DMSO-d_6) δ(ppm): 9.68–9.66 (d, J = 8 Hz, 1H), 8.26–8.23 (d, J = 12 Hz, 1H), 8.19–8.17 (d, J = 8 Hz, 1H), 7.68–7.59 (m, 3H), 7.22 (s, 1H), 6.84 (s, 1H), 4.99–4.93 (m, 1H), 4.61–4.48 (d, J = 52 Hz, 2H), 4.20–4.15 (q, J = 12 Hz, 2H), 4.10–4.07 (t, J = 8 Hz, 2H), 1.62–1.56 (m, 2H), 0.88–0.84 (t, J = 8 Hz, 2H). ^{13}C NMR (150 MHz, DMSO-d_6) δ(ppm): 169.31 (C=O), 163.74 (C=O), 160.26 (ArC), 153.04 (ArC), 138.26 (ArCH), 136.59 (ArC), 128.81 (ArCH), 127.76 (ArC), 127.50 (ArCH), 124.57 (ArCH), 123.60 (ArCH), 120.27 (ArCH), 67.12 (CH_2), 54.05 (CH), 46.00 (CH_2), 21.89 (CH_2), 10.68 (CH_3). ESI-MS m/z: 359.1 $[M+H]^+$; 381.3 $[M+Na]^+$; 357.2 $[M-H]^-$.

4.4.14. Isopropyl 2-(benzo[*d*]thiazole-2-carboxamido)-3-(1*H*-imidazol-1-yl)propanoate (28)

Light white solid; yield: 62.6%; mp: 143.1–144.7 °C. ^{1}H NMR (400 MHz, DMSO-d_6) δ(ppm): 9.64–9.61 (d, J = 12 Hz, 1H), 8.25–8.23 (d, J = 8 Hz, 1H), 8.19–8.17 (d, J = 8 Hz, 1H), 7.72 (s, 1H), 7.68–7.59 (m, 2H), 7.25 (s, 1H), 6.88 (s, 1H), 5.01–4.93 (m, 1H), 4.91–4.87 (m, 1H), 4.57–4.48 (d, J = 36 Hz, 2H), 1.23–1.19 (q, J = 8 Hz, 6H). ^{13}C NMR (150 MHz, DMSO-d_6) δ (ppm): 168.74 (C=O), 163.74 (C=O), 160.23 (ArC), 153.05 (ArC), 138.18 (ArCH), 136.59 (ArC), 128.31 (ArCH), 127.76 (ArC), 127.63 (ArCH), 124.57 (ArCH), 123.59 (ArCH), 120.46 (ArCH), 69.53 (CH), 54.11 (CH), 46.18 (CH_2), 21.91 (2×CH_3). ESI-MS m/z: 359.1 $[M+H]^+$; 381.3 $[M+Na]^+$; 357.2 $[M-H]^-$.

4.4.15. Isobutyl 2-(benzo[*d*]thiazole-2-carboxamido)-3-(1*H*-imidazol-1-yl)propanoate (29)

Light white solid; yield: 62.6%; mp: 147.3–152.6 °C. ^{1}H NMR (400 MHz, DMSO-d_6) δ(ppm): 9.65–9.63 (d, J = 8 Hz, 1H), 8.26–8.24 (d, J = 8 Hz, 1H), 8.19–8.17 (d, J = 8 Hz, 1H), 7.68–7.59 (m, 3H), 7.22 (s, 1H), 6.84 (s, 1H), 4.98–4.93 (m, 1H), 4.57–4.49 (d, J = 32 Hz, 2H), 4.19–4.17 (d, J = 8 Hz, 2H), 1.91–1.82 (m, 1H), 089–0.87 (d, J = 8 Hz, 6H). ^{13}C NMR (150 MHz, DMSO-d_6) δ(ppm): 169.24 (C=O), 163.71 (C=O), 160.31 (ArC), 153.05 (ArC), 138.25 (ArCH), 136.59 (ArC), 128.76 (ArCH), 127.77 (ArC), 127.64 (ArCH), 124.57 (ArCH), 123.61 (ArCH), 120.29 (ArCH), 61.81 (CH), 54.07 (CH), 45.94 (CH_2), 27.68 (CH), 19.17 (2×CH_3). ESI-MS m/z: 373.2 $[M+H]^+$; 395.3 $[M+Na]^+$; 371.2 $[M-H]^-$.

4.5. Metabolic enzymes inhibition assay

The CYP26A1 enzyme inhibitory activity was evaluated using the cell-free microsomal assay as previously described.[13] *HL-60* cells were cultured in RPMI 1640 medium,[37] ATRA was added to the culture medium, then *HL-60* cells were incubated for 12 h before cell harvest. Cells were washed twice with PBS and scraped from plates. Microsomes were prepared by differential centrifugation of homogenized cells. Homogenate was spun at 17,000 g and the supernatant spun again at 100,000 g. The pellet was resuspended in 25 mM potassium phosphate, pH 7.4, 20% v/v glycerol and stored at −80 °C.

Enzymatic assays (HPLC biochemical CYP26A1 assay) were performed in a total volume of 100 μL in a reaction mixture composed of 100 mM Tris pH7.4, 150 mM KCl, 10 mM $MgCl_2$, 2 mM NADPH, 50 nM ATRA, varying concentrations of novel compounds dissolved in ethanol. The final concentration of ethanol in all experiments never exceeded 0.8%. and 50 μg of *HL-60* microsomes. The reactions were incubated at 37 °C for 30 min in the dark. The reaction was quenched with acetonitrile, mixed and spun at 10,000 g for 10 min. The supernatant was removed, ATRA and metabolites were performed with a C18 Waters Spherisorb column with an in-line radiometric detector and detected at 350 nM, and separated by gradient reversed-phase chromatography, using mobile phase A [50% acetonitrile, 50% (0.2%) acetic acid, w/w] and mobile phase B (acetonitrile, 0.1% acetic acid, w/w). A flow rate of 0.3 mL/min was used with linear gradients employed between the specified times as follows: 0, 100% A; 5 min, 100% A; 5.5 min, 40% A,60% B;

12 min, 40% A, 60% B; 12.5 min, 20% A, 80% B; 17.5 min, 20% A, 80% B; 18 min, 100%A; 25 min, 100% A.

Enzymatic assays to measure the inhibition of CYP3A4 activity was determined in 100 μL volume in a 96-well black plate by the use of a fluorescence substrate (BD, Gentest). Compounds were tested at various concentrations in a reaction that contained 200 mM potassium phosphate buffer, pH 7.4, 200 mM NADPH, and 20 μg of CYP3A4. The reaction was incubated at 37 °C for 45 min followed by the addition of 37μL of 80% acetonitrile in 0.5 M Tris base to terminate the reaction. The plates were read at excitation/emission of 405/535 nm, respectively.

Enzymatic assays to measure the inhibition of CYP2D6 activity was determined in 100μL volume in a 96-well black plate by the HPLC biochemical CYP 2D6 assay, The reaction mixture composed of 100 mM Tris pH 7.4, 150 mM KCl, 10 mM $MgCl_2$, 2 mM NADPH, 50 nM ATRA, varying concentrations of novel compounds dissolved in ethanol. The final concentration of ethanol in all experiments never exceeded 0.8%, and 20 μg of CYP2D6. The reaction was incubated at 37 °C for 45 min followedmby the addition of 37μL of 80% acetonitrile in 0.5 M Tris base to terminate the reaction. The plates were read at excitation/emission of 405/535 nm, respectively. Detection method of CYP2D6 consistent with the detection method of CYP26.

4.6. Cell growth inhibition assay

Growth inhibitory activities were evaluated on the CYP26A1 high expression *HL-60* (acute myeloid leukemia) cell line. The effects of the compounds on cell viability were evaluated using the MTT assay. Exponentially growing cells were harvested and plated in 96-well plates at a concentration of 1–104 cells/well. The cells were incubated for 24 h at 37 °C. The cells in the wells were treated with target compounds at the concentration (10 μM) for 48 h. Then, 50 μL MTT (2 mg/mL) was added to each well and incubated for 4 h at 37 °C. After the supernatant was discarded, 150 μL DMSO was added to each well, and the absorbance values were determined using a microplate reader (Bio-Rad Instruments) at 570 nm.

4.7. Cell differentiation-inducing assay

The induced differentiation-inducing activities of the compounds were evaluated using the CYP26A1 high expression *HL60* cell line in vitro with liarozole as the positive control. The cancer cell lines were cultured in standard RPMI-1640 media supplemented with 10% fetal bovine serum (FBS), 100 U/mL penicillin, and 100 μg/mL streptomycin in a humidified atmosphere. Approximately 5×10^5 cells were plated in 24-well plates and incubated in 5% CO_2 at 37 °C for 24 h. The test compounds were added to the culture medium at the indicated final concentrations, and the cell cultures were continued for 72 h. Next, the chromogenic agent (300 μL NBT and 15 μL PMC) was added to each well, and the percent cellular differentiation was calculated as $[Np/(Np + Nn)] \times 100$. Np represents the cell number with the NBT positive results, and Nn represents the cell number with the NBT negative results. All experiments were repeated at least three times.

References and notes

1. Smith, M. A.; Parkinson, D. R.; Cheson, B. D.; Friedman, M. A. *J. Clin. Oncol.* **1992**, *10*, 839.
2. Gudas, L. J.; Wagner, J. A. *J. Cell. Physiol.* **2011**, *226*, 322.
3. Lee, J. S.; Newman, R. A.; Lippman, S. M.; Huber, M. H.; Minor, T.; Raber, M. N.; Krakoff, I. H.; Hong, W. K. *J. Clin. Oncol.* **1993**, *11*, 959.
4. Armstrong, J. L.; Ruiz, M.; Boddy, A. V.; Redfern, C. P. F.; Pearson, A. D. J.; Veal, G. J. *Br. J. Cancer* **2005**, *92*, 696.
5. Ozpolat, B.; Mehta, K.; Berestein, G. L. *Leuk. Lymphoma* **2005**, *46*, 1497.
6. McSorley, L. C.; Daly, A. K. *Biochem. Pharmacol.* **2000**, *60*, 5117.
7. Thacher, S. M.; Vasudevan, J.; Tsang, K. Y.; Nagpal, S.; Chandraratna, R. A. *J. Med. Chem.* **2001**, *44*, 281.
8. Armstrong, J. L.; Boddy, A. V.; Redfern, C. P. F.; Veal, G. J. *Br. J. Cancer* **2007**, *96*, 1675.
9. Marill, J.; Idres, N.; Capron, C. C.; Nguyen, E.; Chabot, G. G. *Curr. Drug Metab.* **2003**, *4*, 1.
10. Yu, Z. C.; Li, J. M.; Shen, Z. X. *Chin. Pharm. J.* **2001**, *12*, 837.
11. Ahmad, M. *Sci. Pharm.* **2011**, *79*, 921.
12. De Coster, R.; Wouters, W.; Van Ginckel, R.; End, D.; Krekels, M.; Coene, M. C.; Bowden, C. *J. Steroid Biochem. Mol. Biol.* **1992**, *43*, 197.
13. Mulvihill, M. J.; Kan, J. L.; Beck, P.; Bittner, M.; Cesario, C.; Cooke, A.; Keane, D. M.; Nigro, A. I.; Nillson, C.; Smith, V.; Srebernak, M.; Sun, F. L.; Vrkljan, M.; Winski, S. L.; Castelhano, A. L.; Emerson, D.; Gibson, N. *Bioorg. Med. Chem. Lett.* **2005**, *15*, 1669.
14. Gomaa, M. S.; Bridgens, C. E.; Aboraia, A. S.; Veal, G. J.; Redfern, C. P. F.; Brancale, A.; Armstrong, J. L.; Simons, C. *J. Med. Chem.* **2011**, *54*, 2778.
15. Stoppie, P.; Borgers, M.; Borghgraef, P.; Dillen, L.; Goossens, J.; Sanz, G.; Szel, H.; Van Hove, C.; Van Nyen, G.; Nobels, G.; Vanden Bossche, H.; Venet, M.; Willemsens, G. J.; Van Wauwe, J. *J. Pharmacol. Exp. Ther.* **2000**, *293*, 304.
16. Van Heusden, J.; Van Ginckel, R.; Bruwiere, H.; Moelans, P.; Janssen, B.; Floren, W.; Van der Leede, B. J.; Van Dun, J.; Sanz, G.; Venet, M.; Dillen, L.; Van Hove, C.; Willemsens, G.; Janicot, M.; Wouters, W. *Br. J. Cancer* **2002**, *86*, 605.
17. Verfaille, C. J.; Thissen, C. A.; Bovenschen, H. J.; Mertens, J.; Steiljen, P. M.; Van De Kerkhof, P. C. M. *J. Eur. Acad. Dermatol. Venereol.* **2007**, *21*, 1038.
18. Verfaille, C. J.; Coel, M.; Boersma, I. H.; Mertens, J.; Borgers, M.; Roseeuw, D. *Br. J. Dermatol.* **2007**, *157*, 122.
19. Geria, A. N.; Scheinfeld, N. S. *Curr. Opin. Investig. Drugs* **2008**, *9*, 1228.
20. Ren, J. H.; Xiong, X. Q.; Sha, Y.; Yan, M. C.; Lin, B.; Wang, J.; Jing, Y. K.; Zhao, D. M.; Cheng, M. S. *Mol. Simul.* **2008**, *34*, 337.
21. Sun, B.; Song, S.; Hao, C. Z.; Huang, W. X.; Liu, C. C.; Xie, H. L.; Lin, B.; Cheng, M. S.; Zhao, D. M. *J. Mol. Graph. Model.* **2015**, *56*, 10.
22. Murray, C. W.; Verdonk, M. L.; Rees, D. C. *Trends Pharmacol. Sci.* **2012**, *33*, 224.
23. Rees, D. C.; Congreve, M.; Murray, C. W.; Carr, R. *Nat. Rev. Drug Disc.* **2004**, *3*, 660.
24. Hubbard, R. E. *J. Synchrotron. Radiat.* **2008**, *15*, 227.
25. Accelrys Software Inc. *Discovery Studio Modeling Environment, Release 4.0*; Accelrys Software: San Diego, 2013.
26. Wolfe, J. P.; Singer, R. A.; Yang, B. H.; Buchwald, S. L. *J. Am. Chem. Soc.* **1999**, *121*, 9550.
27. Zoppellaro, G.; Geies, A.; Enkelmann, V.; Baumgarten, M. *Eur. J. Org. Chem.* **2004**, *11*, 2367.
28. Smolenskii, I. N.; Gontar, S. S.; Markov, V. I.; Mokryi, E. N. *Voprosy Khimii i Khimicheskoi Tekhnologii.* **1986**, *81*, 102.
29. Piotrkowska, B.; Milewska, M. J.; Gdaniec, M.; Polonski, T. *Tetrahedron: Asymmetry* **2007**, *18*, 1486.
30. Lapina, I. M.; Pevzner, L. M. *Russ. J. Gen. Chem.* **2001**, *71*, 1479.
31. Gomaa, M. S.; Armstrong, J. L.; Bobillon, B.; Veal, G. J.; Brancale, A.; Redfern, C. P. F.; Simons, C. *Bioorg. Med. Chem.* **2008**, *16*, 8301.
32. Li, F. R.; Zhao, D. M.; Ren, J. H.; Hao, F. Y.; Liu, G. Y.; Jin, S. F.; Jing, Y. K.; Cheng, M. S. *Bioorg. Med. Chem.* **2013**, *21*, 3256.
33. Zhao, D. M.; Sun, B.; Ren, J. H.; Li, F. R.; Song, S.; Lv, X. J.; Hao, C. Z.; Cheng, M. S. *Bioorg. Med. Chem.* **2015**, *23*, 1356.
34. Rendic, S.; Di Carlo, F. *Drug Metab. Rev.* **1997**, *29*, 413.
35. Wang, A.; Stout, C. D.; Zhang, Q.; Johnson, E. F. *J. Biol. Chem.* **2015**.
36. Branden, G.; Sjogren, T.; Schnecke, V.; Xue, Y. *Drug Discovery Today* **2014**, *19*, 905.
37. Chang-hai, L. *Chin. J. Cell Mol. Immunol.* **2005**, *21*, 637.